Reconciling plate kinematic and seismic estimates of lithospheric convergence in the central Indian Ocean

J.M. Bull[1], C. DeMets[2], K.S. Krishna[3], D.J. Sanderson[4], and S. Merkouriev[5]

[1]School of Ocean and Earth Science, National Oceanography Centre Southampton, University of Southampton, Southampton SO14 3ZH, UK

[2]Department of Geoscience, University of Wisconsin-Madison, Madison, Wisconsin 53706, USA

[3]National Institute of Oceanography, Council of Scientific and Industrial Research, Dona Paula, Goa 403004, India

[4]School of Civil Engineering and the Environment, University of Southampton, Southampton SO17 1BJ, UK

[5]St. Petersburg Filial of Institute of Terrestrial Magnetism, Ionosphere and Radio Wave Propagation (SPbFIZMIRAN), Muchnoj per, 2, Box 188, St. Petersburg, Russia

ABSTRACT

The far-field signature of the India-Asia collision and history of uplift in Tibet are recorded by sediment input into the Indian Ocean and the strain accumulation history across the diffuse plate boundary between the Indian and Capricorn plates. We describe the history of India-Capricorn convergence from updated estimates of India-Somalia-Capricorn plate rotations and observations derived from seismic reflection data. New India-Capricorn plate rotations for the past 20 m.y. are consistent with slow north-south convergence from 18 Ma about a stationary or nearly stationary pole near the eastern edge of the Chagos-Laccadive ridge, simpler than predicted by previous models based on many fewer data. The new rotations suggest that convergence began between 18 and 14 Ma, consistent with marine seismic evidence for an onset of deformation at 15.4–13.9 Ma. They further show that convergence rates doubled at 8 Ma, in agreement with a sharp increase in fault activity at 8–7.5 Ma seen on seismic reflection profiles. A discrepancy between the total strain estimated from kinematic and seismic reflection data can be reconciled if pervasive reverse faulting within the diffuse plate boundary is accompanied by block rotations of 1°–3°.

INTRODUCTION

The deformation zone within the central Indian Ocean is the best-studied diffuse plate boundary zone in the oceans (Fig. 1). The deformation is manifest on two spatial scales: reverse faulted blocks with 5–10 km spacing, and 100–300-km-wavelength folding of the oceanic lithosphere. The deformation has been described by seismic reflection, heat flow, studies of intraplate seismicity, and satellite gravity studies (e.g., Weissel et al., 1980; Bull and Scrutton, 1990a; Chamot-Rooke et al., 1993; Deplus et al., 1998; Delescluse et al., 2008; Delescluse and Chamot-Rooke, 2007). Motion across the diffuse plate boundary zone has been estimated independently from inversions of seafloor spreading rates and directions from the Carlsberg and Central Indian ridges and consists of counterclockwise rotation about a pole east of Chagos Bank (Royer and Gordon, 1997; Gordon et al., 1998; DeMets et al., 2005), such that convergence is predicted in the Central Indian and Wharton Basins, and extension west of Chagos Bank.

Seismic stratigraphic analysis of the Bengal Fan sediments has revealed that the main deformation phase began in the Miocene (8.0–7.5 Ma; Cochran, 1990) and included long-wavelength folding, development of a regional unconformity, pervasive reverse faulting, with continuation of long-wavelength folding and faulting in the Pliocene (5.0–4.0 Ma) and Pleistocene (0.8 Ma) (Krishna et al., 2001). Plate reconstructions independently confirm the onset of rapid deformation at 8–7 Ma (DeMets et al., 2005), and moreover suggest that significant, but slower deformation began as early as 20 Ma with large uncertainties. Seismic stratigraphic data (Krishna et al., 2009) suggest that slow deformation began at 15.4–13.9 Ma.

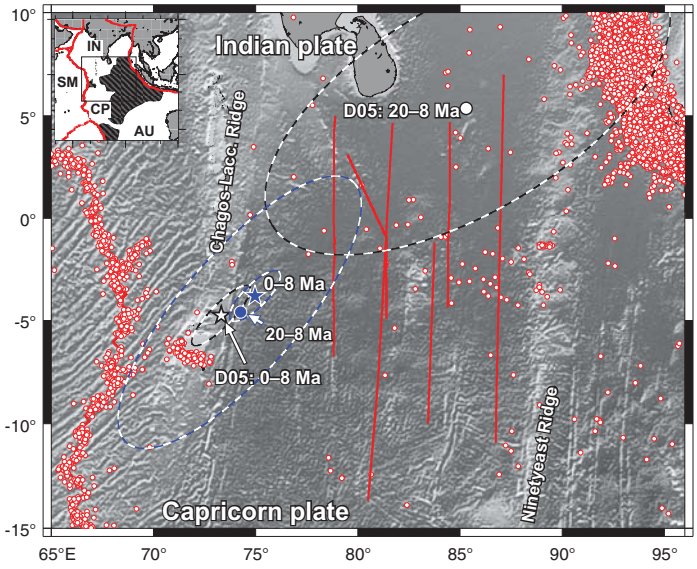

Figure 1. Location map of study area. Red circles show shallow earthquakes from 1963 to 2008, all magnitudes, from U.S. National Earthquake Information Center database. Red lines show locations of seismic profiles described in text. Solid blue star and circle show 8–0 Ma and 20–8 Ma Capricorn-India pole locations for this study, respectively. White star and circle labeled D05 show Capricorn-India 8–0 Ma and 20–8 Ma poles from DeMets et al. (2005). Ellipses show two-dimensional, 1σ uncertainties. Inset shows extent of major plates and diffuse plate boundaries (stripes); CP—Capricorn; IN—India; SM—Somalia; AU—Australia.

Although previous independent analyses of seismic stratigraphic and plate kinematic data from the central Indian Ocean confirm important aspects of the style and timing of deformation across the wide plate boundary south of India, important discrepancies and uncertainties remain. For example, the most recent model for India-Capricorn plate motion (DeMets et al. 2005) predicts a systematic increase in the magnitude of north-south shortening across the India-Capricorn boundary zone east of the pole of rotation, whereas a recent analysis of seismic reflection data suggests a more complex pattern (Krishna et al., 2009). Cumulative north-south strain smaller than predicted from plate rotations has been found (Krishna et al., 2009), suggesting that unaccounted errors exist in one or both estimates, or that some deformation occurs either outside the diffuse boundary or via mechanisms not considered in these studies.

Here we derive new India-Capricorn finite rotations for the past 20 m.y. from recently published, high-resolution India-Somalia and Capricorn-Somalia rotations. We then compare these predictions with new

shortening estimates from seismic reflection data that are based on rotations of reversely faulted blocks.

UPDATED PLATE KINEMATIC ESTIMATE

The new India-Capricorn-Somalia rotations (Tables DR1–DR3 in the GSA Data Repository[1]) are derived from new high-resolution estimates of India-Somalia motion since 20 Ma (Merkouriev and DeMets, 2006) and Capricorn-Somalia finite rotations (from DeMets et al., 2005). The India-Somalia rotations are determined from an order-of-magnitude more magnetic anomaly crossings than those of DeMets et al. (2005) and describe a simpler and better constrained post–20 Ma kinematic history than prior models. We corrected both sets of rotations for the effect of outward displacement, which shifts the midpoints of magnetic reversals several kilometers outward from spreading axes due to the finite width of the zone in which new seafloor acquires its magnetization (DeMets and Wilson, 2008). Information about the methods used to estimate the new rotations is given in the Data Repository.

Interval spreading rates determined from the updated Capricorn-Somalia and India-Somalia rotations (Fig. DR1) illustrate the primary kinematic evidence for a change in India and Capricorn plate motions at 8–10 Ma, as discussed by Merkouriev and DeMets (2006). Spreading rates along both boundaries decreased by 25%–30% from 20 Ma to ca. 10 Ma, and then remained steady or increased slightly to the present. The newly estimated interval rates are less noisy than their predecessors (Merkouriev and DeMets, 2006) and clearly suggest two distinct stages of motion for both plate pairs since 20 Ma.

The new best-fitting India-Capricorn poles (Fig. 2; Table DR3) are all located within several hundred kilometers of the eastern edge of the Chagos-Laccadive ridge and show no dependence on age. For example, the rotations that describe motion from the present to 8 Ma and from 8 to 20 Ma (Fig. 1) differ insignificantly in location and predict that approximate north-south shortening dominated deformation nearly everywhere along the plate boundary during their respective time intervals. In contrast, the 20–8 Ma pole determined from rotations in DeMets et al. (2005) is 1200 km northeast of the 8–0 Ma estimate (Fig. 1) and predicts a component of extension across more than two-thirds of the India-Capricorn boundary before 8 Ma, in conflict with evidence for shortening at that time (Krishna et al., 2009). The new India-Capricorn rotation estimates therefore yield a simpler kinematic history that agrees better with the independently determined shortening history across the diffuse plate boundary than was previously the case.

We interpret the new results as evidence that India-Capricorn motion since 20 Ma is well described by a stationary pole (at 3.7°S, 74.8°E in Fig. 1) located at the Fisher mean of the best-fitting rotations. That the stationary pole is near the eastern edge of the Chagos-Laccadive ridge, which consists of unusually thick oceanic crust formed by the Reunion mantle plume (Henstock and Thompson, 2004), may indicate that the ridge plays a mechanical role in determining the pole location.

Using the stationary India-Capricorn pole described above, we apply procedures described by DeMets et al. (2005) to estimate an optimized time sequence of rotation angles (upper panel of Fig. 2). The new sequence of angles can be interpreted as evidence for either a two-stage or three-stage rotation history. Both include the previously reported factor of two increase in India-Capricorn motion since 8 Ma (DeMets and Royer, 2003; DeMets et al., 2005), and the three-stage rotation history subdivides motion before 8 Ma into periods of slow or possibly no motion before ca. 16 ± 2 Ma and somewhat faster motion from ca. 16 ± 2 Ma to 8 Ma.

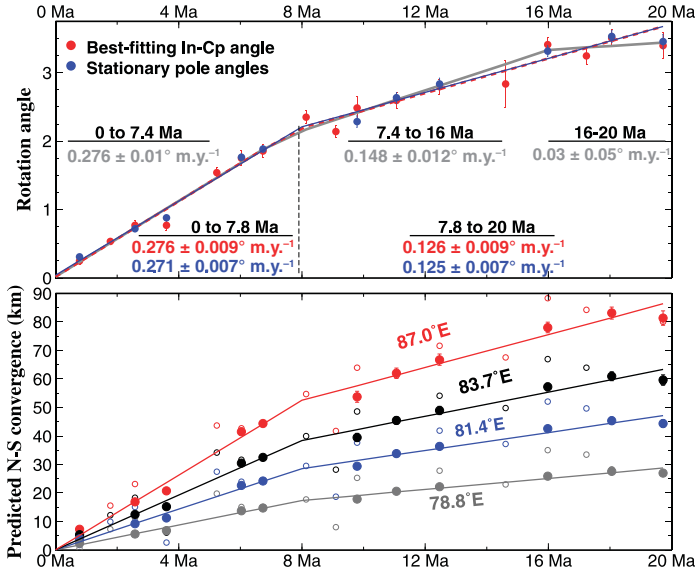

Figure 2. Upper: India-Capricorn (In-Cp) finite rotation angles and standard errors for best-fitting poles from Table DR4 (see footnote 1) and for 0–20 Ma stationary pole at 3.74°S, 74.76°E. Stationary pole angles are procedurally limited to magnetic reversals for which identical crossing points were used to reconstruct Capricorn-Somalia (DeMets et al. 2005) and India-Somalia (Merkouriev and DeMets, 2006) plate positions. Gray lines indicate best-fitting three-stage rotation history described in text. Red and blue lines show best-fitting, least-squares two-stage history for both sets of rotation angles. Ages for changes in motion were estimated as part of inversion procedure and give a best age of 7.8 ± 1 Ma. Lower: Predicted north-south shortening component across India-Capricorn plate boundary, 0–20 Ma. Shortening is predicted at 3.5°S at longitudes of four seismic profiles shown in Figure 1. Filled and open symbols are derived from stationary-pole and best-fitting India-Capricorn rotations, respectively.

Inversions of the angles in Figure 2 to estimate best-fitting slopes and ages for changes in motion for the two- and three-stage models indicate that a motion change at 7.8 Ma is highly significant, but that any earlier change cannot be distinguished reliably from the sparse and less certain angles for times before 13 Ma.

SEISMIC REFLECTION ANALYSIS

In the most recent synthesis of seismic reflection data (Krishna et al., 2009), measurements were made on the vertical separations of sedimentary horizons and unconformities on either side of 293 reverse faults. These data were then backstripped to determine fault activity histories. These data indicate that near or prior to 20 Ma, isolated faults accommodated minor extensional movement before a period of tectonic quiescence. Compressional activity then began on individual fault blocks at 15.4–13.9 Ma and continued to 8.0–7.5 Ma. Strain rates increased abruptly at 8.0–7.5 Ma, which led to widespread reverse faulting and the formation of long-wavelength undulations and the first regional unconformity, and have continued to present.

Previously, workers calculated the cumulative shortening accommodated by reverse faulting across the diffuse plate boundary (Chamot-Rooke et al., 1993; Van Orman et al., 1995; Krishna et al., 2009) using a three-stage procedure. Vertical separations of sedimentary reflectors immediately above basement are first measured and depth converted using the velocity law in Bull and Scrutton (1990b). These were assumed to approximate fault throws, and the horizontal (shortening) component was calculated using dips (36°–45°) for the reverse faults in the top of the

[1]GSA Data Repository item 2010083, supplementary tables, figures, and information on new India-Capricorn-Somalia rotations, is available online at www.geosociety.org/pubs/ft2010.htm, or on request from editing@geosociety.org or Documents Secretary, GSA, P.O. Box 9140, Boulder, CO 80301, USA.

oceanic crust estimated from the seismic reflection data (e.g., Bull and Scrutton, 1992; Chamot-Rooke et al., 1993). This approach has yielded total strain estimates of 1.9%–4.3% across the diffuse boundary. Long-wavelength undulations in the central Indian Ocean accommodate <1% of the total shortening across the diffuse plate boundary and are thus ignored in the following.

The procedure outlined above has three limitations that are likely to produce underestimates of the shortening: (1) the vertical separations are made in poorly imaged regions above and below the fault surface and incorporate drag; (2) the vertical separation is less than the throw for dipping horizons; and (3) the method ignores the likely contribution of fault block rotation to the estimated shortening. In the Central Indian Basin, seismic reflection data from faulted blocks (Fig. 3) clearly show that the top of layer 2 is rotated by 1°–3° relative to horizontal (Fig. 3A), with some fault blocks rotated by 6°–8° (Fig. 3B). Previously published shortening estimates may thus underestimate the total shortening across the diffuse plate boundary.

We therefore recalculated shortening due to reverse faulting by applying a method widely used for rotational extensional faults, the "domino" model of Wernicke and Burchfiel (1982). This provides an independent estimate of shortening without the problems inherent in determining heave from cutoffs at faults, and incorporates the observed rotations. The method requires an estimate of the dip of each reverse fault and the rotation of each fault block (Fig. 3C), which can be approximated by the dip of the top of the oceanic crust. Reliable measurements of the latter are only feasible with multichannel seismic reflection data, which consistently image the top of basement (Bull and Scrutton, 1992; Chamot-Rooke et al., 1993). Multichannel data coverage is, however, much sparser than the single-channel data synthesized by Van Orman et al. (1995) and Krishna et al. (2009), thereby precluding an observationally based correction for each fault that has been imaged in the diffuse plate boundary. We therefore reestimated the total shortening for a range of plausible fault block rotations (ω = 1°–3°), an average fault dip (δ) of 40°, and using profile lengths at each longitude defined by the distance between the most widely distributed faults (see Krishna et al., 2009). These give revised shortening estimates of 2.1% to 6.4%, which result in between 17 and 52 km of north-south convergence at 78.8°E, increasing eastward to between 34 and 104 km of convergence at 87°E (Fig. 4). The higher value exceeds previous maximum shortening estimates from seismic reflection data, most likely due to the problems described here in measuring vertical displacement across faults.

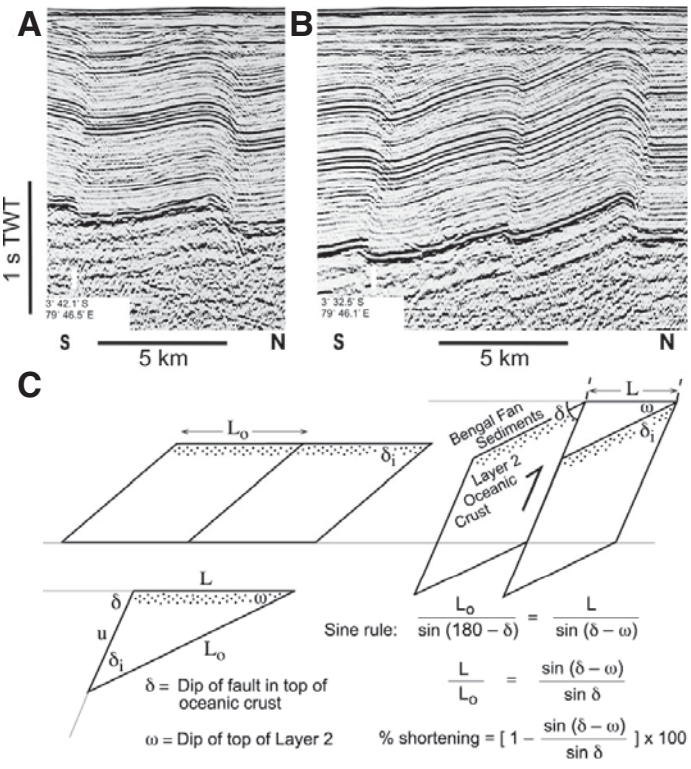

Figure 3. Seismic reflection images of tilted fault blocks bounded by reverse faults and the simple geometrical construction used to calculate shortening. A: Fault block (representative of deformational area) with dip on top of layer 2 of 2°–3°. TWT—two-way traveltime. B: Fault blocks showing maximum amount of rotation with dip on top of layer 2 of 4°–8°. Calculations of fault dip use velocity law of Bull and Scrutton (1990b). C: Simple geometrical construction used to calculate shortening based solely on dip of reverse faults in upper part of oceanic crust (δ), and dip of top of oceanic crust layer 2 (ω) (see text for discussion). L—fault block width; L_0—original fault block width.

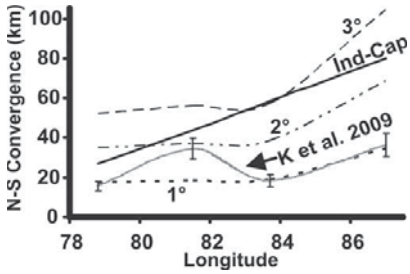

Figure 4. Cumulative shortening since 20 Ma predicted by new fixed-pole model for India-Capricorn (Ind-Cap) motion (black line) compared to simple geometrical models for different angles of fault block rotation (Fig. 3), and previous estimates of shortening derived from seismic reflection data assuming average reverse fault dips of 40° in the oceanic crust. 1°, 2°, and 3° refer to dip of top of oceanic layer 2 (ω in Fig. 3C). Error bars indicate range for observed fault dips 36°–45° (Krishna et al., 2009; in figure, K et al., 2009).

SYNTHESIS AND CONCLUSIONS

Here we summarize where our new plate kinematic analysis (Fig. 2) reconciles previous differences with seismic stratigraphic studies, and where differences remain. There is striking agreement concerning the acceleration of convergence and associated contractional deformation at 8 Ma, with a well-defined factor of two increase in the rate of angular rotation contemporaneous with the development of a regional unconformity related to the formation of long- wavelength (100–300 km) folds, and an increase in reverse faulting activity seen on the seismic reflection profiles (Krishna et al., 2009). Both methods agree that convergence (and associated contractional deformation) began earlier, and more slowly, than at 8 Ma. We show how a simple rotational model for reverse fault blocks can be used to reconcile the total amount of convergence across the diffuse plate boundary zone.

Additional work is needed to better resolve the history of India-Capricorn motion before 10 Ma. Whereas seismic stratigraphic–derived estimates indicate that convergence began at 15.4–13.9 Ma, the India-Capricorn rotation history allows for an onset of convergence as early as 18 Ma (Fig. 2). A conservative interpretation of these results is that slow convergence began between 18 and 13.9 Ma. Better stratigraphic age control from future Integrated Ocean Drilling Program (IODP) study sites in the Bengal Fan is needed to reduce the uncertainty in our stratigraphic estimate, which relies on extrapolation of rates from a single drill site (ODP Leg 116). Analyses of additional magnetic anomalies are needed to improve the limited temporal resolution and uncertainties for rotations for times before 13 Ma, as well as test whether the negative rotation angle from 20 to 18 Ma, coinciding with a period of possible normal faulting observed by Krishna et al. (2009), is supported by additional reconstructions. Our new kinematic estimates do not reveal possible discrete phases

of deformation at 5.0–4.0 Ma and 0.8 Ma inferred from seismic reflection data (Krishna et al. 2001), and are instead most simply interpreted as consistent with steady motion about a fixed pole since ca. 8 Ma (Fig. 2).

The cumulative shortening estimate of Krishna et al. (2009) from seismic reflection data (Fig. 4) is smaller than predicted by our updated and previous kinematic models for all four of the seismic profiles included in their analysis (Fig. 4), with differences of ~40 km for two profiles that greatly exceed the estimated uncertainties (±10 km). Given that all four profiles span almost all of the most intensely deforming areas of the plate boundary (Fig. 1), it seems unlikely that the discrepancy between the two independent shortening estimates can be attributed to structures not imaged by the seismic profiles. Similarly, the plate kinematic estimates are based on numerous unambiguous magnetic and bathymetric data, and are both robust and have well-characterized uncertainties.

We demonstrate here that previous shortening estimates from seismic reflection data were too low. Our new estimates of total shortening for assumed average fault block rotations of 2°–3° and average fault dips of 40° (Fig. 4) bracket the shortening estimates predicted by our updated kinematic model, and thus fully reconcile the two independent estimates. Although not all the fault blocks show evidence for rotation, and some fault blocks (e.g., Fig. 3B) are rotated more than 3°, we find it encouraging that such a simple geometric model can resolve the previously large discrepancy between the shortening estimates.

Reasons for the onset of convergence at 18–14 Ma are unclear, as are the causes of the sharp increase in deformation at 8 Ma: we know of no significant changes in spreading rates or directions at the Indian Ocean ridge system at these times. We follow others (e.g., Molnar and Stock, 2009; Gordon, 2009) in suggesting that the answers must lie within the history of Tibet, the uplift of which caused increased deviatoric stresses over a wide area, including the equatorial Indian Ocean. We note that a recent analysis of motion between the Indian and Eurasian plates (Molnar and Stock, 2009), although having less temporal resolution than our study, is consistent with an event at 17 Ma causing a slowing of India-Eurasia convergence. That the India-Capricorn rotation pole since ca. 18 Ma has remained stationary and adjacent to the Chagos-Laccadive ridge may indicate that the ridge played a mechanical role in determining the pole location and hence deformation across the wide equatorial plate boundary.

ACKNOWLEDGMENTS

We thank the Council of Scientific and Industrial Research and the Royal Society of London for their support. We thank Richard Gordon, Laurent Montesi, Patience Cowie, and an anonymous reviewer for their careful and constructive comments, which significantly improved the manuscript. We are grateful to Steve Cande and Dave Rowley for changes they recommended to the Data Repository materials.

REFERENCES CITED

Bull, J.M., and Scrutton, R.A., 1990a, Fault reactivation in the central Indian Ocean and the rheology of oceanic lithosphere: Nature, v. 344, p. 855–858, doi: 10.1038/344855a0.

Bull, J.M., and Scrutton, R.A., 1990b, Sediment velocities and deep structure from wide-angle reflection data around Leg 116 sites, *in* Cochran, J.R., et al., Proceedings Ocean Drilling Program, Scientific results, Volume 116: College Station, Texas, Ocean Drilling Program, p. 311–316.

Bull, J.M., and Scrutton, R.A., 1992, Seismic reflection images of intraplate deformation, central Indian Ocean, and their tectonic significance: Geological Society of London Journal, v. 149, p. 955–966, doi: 10.1144/gsjgs.149.6.0955.

Chamot-Rooke, N., Jestin, F., de Voogd, B., and Phedre Working Group, 1993, Intraplate shortening in the central Indian Ocean determined from a 2100-km-long north-south deep seismic reflection profile: Geology, v. 21, p. 1043–1046, doi: 10.1130/0091-7613(1993)021<1043:ISITCI>2.3.CO;2.

Cochran, J.R., 1990, Himalayan uplift, sea level, and the record of Bengal Fan sedimentation at the ODP Leg 116 sites, *in* Cochran, J.R., et al., Proceedings of the Ocean Drilling Program, Scientific results, Volume 116: College Station, Texas, Ocean Drilling Program, p. 397–414.

Delescluse, M., and Chamot-Rooke, N., 2007, Instantaneous deformation and kinematics of the India-Australia plate: Geophysical Journal International, v. 168, p. 818–842, doi: 10.1111/j.1365-246X.2006.03181.x.

Delescluse, M., Montési, L.G.J., and Chamot-Rooke, N., 2008, Fault reactivation and selective abandonment in the oceanic lithosphere: Geophysical Research Letters, v. 35, L16312, doi: 10.1029/2008GL035066.

DeMets, C., and Royer, J.-Y., 2003, A new high-resolution model for India-Capricorn motion since 20 Ma: Implications for the chronology and magnitude of distributed crustal deformation in the Central Indian Basin: Current Science, v. 85, p. 339–345.

DeMets, C., and Wilson, D.S., 2008, Toward a minimum change model for recent plate motions: Calibrating seafloor spreading rates for outward displacement: Geophysical Journal International, v. 174, p. 825–841, doi: 10.1111/j.1365-246X.2008.03836.x.

DeMets, C., Gordon, R.G., and Royer, J.-Y., 2005, Motion between the Indian, Capricorn and Somalian plates since 20 Ma: Implications for the timing and magnitude of distributed lithospheric deformation in the equatorial Indian Ocean: Geophysical Journal International, v. 161, p. 445–468, doi: 10.1111/j.1365-246X.2005.02598.x.

Deplus, C., Diament, M., Hebert, H., Bertrand, G., Dominguez, S., Dubois, J., Malod, J., Patriat, P., Pontoise, B., and Sibilla, J.J., 1998, Direct evidence of active deformation in the eastern Indian oceanic plate: Geology, v. 26, p. 131–134, doi: 10.1130/0091-7613(1998)026<0131:DEOADI>2.3.CO;2.

Gordon, R.G., 2009, Lithospheric deformation in the equatorial Indian Ocean: Timing and Tibet: Geology, v. 37, p. 287–288, doi: 10.1130/focus032009.1.

Gordon, R.G., DeMets, C., and Royer, J.-Y., 1998, Evidence for long-term diffuse deformation of the lithosphere of the equatorial Indian Ocean: Nature, v. 395, p. 370–374, doi: 10.1038/26463.

Henstock, T.J., and Thompson, P.J., 2004, Self-consistent modeling of crustal thickness at Chagos-Laccadive Ridge from bathymetry and gravity data: Earth and Planetary Science Letters, v. 224, p. 325–336, doi: 10.1016/j.epsl.2004.05.021.

Krishna, K.S., Bull, J.M., and Scrutton, R.A., 2001, Evidence for multiphase folding of the central Indian Ocean lithosphere: Geology, v. 29, p. 715–718, doi: 10.1130/0091-7613(2001)029<0715:EFMFOT>2.0.CO;2.

Krishna, K.S., Bull, J.M., and Scrutton, R.A., 2009, Early (pre-8 Ma) fault activity and temporal strain accumulation in the central Indian Ocean: Geology, v. 37, p. 227–230, doi: 10.1130/G25265A.1.

Merkouriev, S., and DeMets, C., 2006, Constraints on Indian plate motion since 20 Ma from dense Russian magnetic data: Implications for Indian plate dynamics: Geochemistry Geophysics Geosystems, v. 7, Q02002, doi: 10.1029/2005GC001079.

Molnar, P., and Stock, J.M., 2009, Slowing of India's convergence with Eurasia since 20 Ma and its implications for Tibetan mantle dynamics: Tectonics, v. 28, TC3001, doi: 10.1029/2008TC002271.

Royer, J.-Y., and Gordon, R.G., 1997, The motion and boundary between the Capricorn and Australian plates: Science, v. 277, p. 1268–1274, doi: 10.1126/science.277.5330.1268.

Van Orman, J., Cochran, J.R., Weissel, J.K., and Jestin, F., 1995, Distribution of shortening between the Indian and Australian plates in the central Indian Ocean: Earth and Planetary Science Letters, v. 133, p. 35–46, doi: 10.1016/0012-821X(95)00061-G.

Weissel, J.K., Anderson, R.N., and Geller, C.A., 1980, Deformation of the Indo-Australian plate: Nature, v. 287, p. 284–291, doi: 10.1038/287284a0.

Wernicke, B., and Burchfiel, B.C., 1982, Modes of extensional tectonics: Journal of Structural Geology, v. 4, p. 105–115, doi: 10.1016/0191-8141(82)90021-9.

Manuscript received 10 July 2009
Revised manuscript received 24 October 2009
Manuscript accepted 27 October 2009

Printed in USA

Digital Repository 2010083: Supplementary tables and information

"Reconciling plate kinematic and seismic estimates of lithospheric convergence in the central Indian Ocean"

by J. M. Bull, C. DeMets, K. S. Krishna, D. J. Sanderson, and S. Merkouriev

Overview

This supplementary document describes the India-Capricorn-Somalia rotations that are used for the analysis presented in the accompanying *Bull et al.* paper and includes rotations that supersede those published in previous related studies. Updated Capricorn-Somalia and India-Somalia finite rotations and the methods used to estimate them are described first. Rotations modified for the influence of outward displacement are then presented and used as the basis for a synopsis of key kinematic results.

The estimated magnetic reversal ages are given in the tables and are from the astronomically tuned Neogene time scale of *Lourens et al.* (2004) for reversals younger than 7.2 Ma and older than 15.2 Ma. For reversals between these two times, we adopt more recently, astronomically-tuned reversal ages from *Husing et al.* (2007) and *Husing* (2008).

Capricorn-Somalia finit rotations

Finite rotations from *DeMets et al.* (2005) for twenty magnetic reversals from the present back to the old edge of Anomaly 6 (19.72 Myr) constitute the starting basis for our new Capricorn-Somalia rotations. Fourteen of the twenty magnetic reversals that were used by *DeMets et al.* (2005) to determine Capricorn-Somalia motion are correlated at the same point on the magnetic anomaly waveform as was used by *Merkouriev and DeMets* (2006) for their analysis of India-Somalia motion. Six additional reversals that were also used in both studies were correlated at slightly different points on the anomaly waveforms and therefore measure the plate motions at different times. For example, anomaly 4n.2 was correlated at its mid-point (7.915 Myr) by *DeMets et al.* (2005), but at its old edge (8.132 Myr) by *Merkouriev and DeMets* (2006). We eliminated these small inconsistencies between the two studies by either increasing or decreasing the Capricorn-Somalia rotation angles from *DeMets et al.* (2005) to compensate exactly for the age difference in the magnetic reversal tie points that were used in the two studies. DR Table 1 lists the updated Capricorn-Somalia finite rotations, including these angular adjustments.

Updated India-Somalia rotations

The updated India-Somalia finite rotations (DR Table 2) are similar to, but updated from finite rotations for reversals C1n through C6no described by *Merkouriev and DeMets* (2006). All of the new rotations are determined from the same magnetic anomaly crossings as were used by *Merkouriev and DeMets* (2006). In addition, the rotations for anomalies 1 to 5Cn.3 were determined using the same fracture zone crossings as were used by *Merkouriev and DeMets* (2006). For Chrons 5D, 5E, and 6no, we elected to use revised sets of fracture zone crossings to estimate the new best-fitting finite rotations because two fracture zones that were selected by *Merkouriev and*

DeMets for those three reversals may have been affected by slow propagating rifts that were active near the paleo-ridge axis.

For Chrons 5D and 5E, the new best-fitting rotations differ by only 0.01-0.02 angular degrees in location and 0.001-0.002 degrees in opening angle from those estimated by *Merkouriev and DeMets* (2006). The updated rotation for C6no however lies 0.6 angular degrees south of the *Merkouriev and DeMets* estimate, closer to and hence more consistent with the opening poles for Chron 5D and 5E than was previously the case. The revised set of fracture zone crossings that are used to estimate the revised best-fitting rotation for Chron 6no have lower dispersion relative to small circles around the new rotation than was previously the case. Both suggest that the updated rotation more accurately describes motion since Chron 6no than that of *Merkouriev and DeMets* (2006).

We also reestimated the uncertainties for all 20 India-Somalia rotations using a bootstrapping methodology that differs modestly from the bootstrapping technique used by *Merkouriev and DeMets* (2006). From the full pool of magnetic anomaly and fracture zone segments that we used to reconstruct each magnetic reversal, we extracted separate random samples of the fracture zone segments and paleo-spreading segments, combined all magnetic anomaly and fracture zone crossings from those randomly sampled segments, and then inverted the combined data to determine the best-fitting bootstrap rotation for that sample. After repeating this procedure one thousand times per reversal to sample the underlying data variations, we used the resulting distribution of rotations to define the rotation uncertainties.

The procedure used by *Merkouriev and DeMets* (2006) differs from the above procedure in one respect. *Merkouriev and DeMets* constructed each bootstrap data sample by repeated random sampling of the combined pool of fracture zone and paleo-spreading segments. Because some reversals included as few as three fracture zone segments, some of their bootstrap samples excluded all fracture zone data. Inversions of those samples yielded poorly determined rotations that were outliers in the distribution of bootstrap rotations. These outliers gave rise to overly large estimates of the covariances for some rotations and unduly pessimistic rotation uncertainties. Our newly estimated rotation variances are 10%-50% smaller than their previous estimates from *Merkouriev and DeMets* (2006). Both the finite rotations and covariances listed in DR Table 2 supersede those from *Merkouriev and DeMets* (2006).

India-Capricorn-Somalia rotations corrected for outward displacement

Outward displacement of the mid-points of magnetic reversals due to the finite width of the zone in which new seafloor acquires its magnetization biases estimates of finite rotations, as described by *DeMets and Wilson* (2008) and *Merkouriev and DeMets* (2008). We therefore corrected both the Capricorn-Somalia and India-Somalia finite rotations given in DR Tables 1 and 2 for the likely influence of outward displacement by adding to each best-fitting rotation a counter-rotation that removes the estimated outward displacement for each of these plate pairs. For the Capricorn-Somalia plate pair, outward displacement averages 2.0 km (*DeMets and Wilson* (2008) and was removed by adding to each Capricorn-Somalia best-fitting rotation an opposite sense small-angle rotation of 0.018^o about a pole located at 55.3^oN, 5.3^oE. Doing so removes 2.0 km of net ridge-normal opening everywhere along plate boundary and yields the best corrected estimate of plate motion for this plate pair. From detailed analyses of magnetic anomaly crossings from the Carlsberg and northern Central Indian ridges, *Merkouriev and DeMets* (2008) and *DeMets and Wilson* (2008) find evidence for uniform outward displacement of 3.5 km. We corrected for this bias by adding to each India-Somalia best-fitting rotation an opposite sense small-angle rotation of 0.032^o

about a pole located at 32.7^{o}N, 330.9^{o}E. This removes 3.5 km of net ridge-normal opening everywhere along plate boundary.

The Capricorn-Somalia and India-Somalia rotations that are corrected for outward displacement are given in DR Table 3 and are referred to hereafter as plate motion rotations since they specify plate motions free from the bias introduced by outward displacement. The rotations are corrected assuming that the magnitude of outward displacement is the same for all paleo-spreading segments. Although significant along-axis variations in outward displacement occur along other spreading centers (*DeMets and Wilson* 2008) and therefore add uncertainty to the corrected rotation estimates, our bootstrapping procedure implicitly accounts for such variations. The bootstrapped rotation uncertainties in DR Tables 1 and 2 are therefore appropriate for the rotations given in DR Table 3.

India-Capricorn plate motion rotations are determined from the Capricorn-Somalia and India-Somalia rotations (DR Table 4) and are the basis for the kinematic analysis presented in the accompanying paper. We next summarize the principal kinematic results from the newly estimated rotations.

Kinematic synopsis

DR Figures 1 and 2 summarize the primary results from the updated Capricorn-Somalia-India rotations given in DR Tables 3 and 4. The interval seafloor spreading rates for the Capricorn-Somalia and India-Somalia plate pairs define a period of decelerating seafloor spreading from 20 Ma to 10 Ma (DR Fig. 1), following by a period of remarkably constant seafloor spreading from 8 Ma to the present, as reported by *Merkouriev and DeMets* (2006). Differences in these and the previously reported interval rates are attributable to the systematic correction for outward displacement that is applied to all of the rotations herein and the revisions to the magnetic reversal ages that define the ages that bracket these interval rates.

Relative to the interval rates previously reported by *Merkouriev and DeMets* (shown by the open symbols in DR Fig. 2), the newly estimated interval rates (solid symbols in DR Fig. 2) exhibit less variation and hence more consistency from one interval to the next. The reduced scatter suggests that the updated rotations are more accurate than those presented by *Merkouriev and DeMets* (2006).

The India-Capricorn poles exhibit no obvious inter-dependence between their ages and their locations (upper panel of DR Fig. 2), and instead tend to scatter relatively evenly around a mean location near 3.7^{o}S, 74.8^{o}E. Differences in the locations of poles of different ages are generally insignificant and are attributable to noise in the underlying India-Somalia and Capricorn-Somalia rotation estimates. The India-Capricorn pole that describes motion from the present back to 8 Ma (labeled "4n.2" in DR Fig. 2), during a period when India-Capricorn-Somalia plate motions appear to have remained constant or nearly constant (*DeMets et al.* 2005; *Merkouriev and DeMets* 2006), is nearly coincident with the pole for the present back to 20 Ma (labeled "6no" in DR Fig. 2). There is thus little evidence for a significant change in the direction of India-Capricorn motion since 20 Ma.

The India-Capricorn rotation angles (lower panel of DR Fig. 2) clearly indicate that the rate of angular rotation changed once and possibly twice since 20 Ma. We therefore examined the fits of two models to the rotation angles, one that postulates a single change in the angular rotation rate since 20 Ma and the other two such changes.

For a single assumed change in the angular rotation rate, we searched systematically for the age that gives the best weighted least-squares, two-line fit to the series of rotation angles and

their assigned reversal ages, including an angle of 0.0 degrees at 0.0 Ma. For each age that we assumed the change took place, we inverted the India-Capricorn angles from DR Table 4 to find the continuous two segment line, consisting of two slopes and one Y-intercept, that best fits the angles and their uncertainties. An inversion in which the angular rotation rate is assumed to have changed at 7.8 Ma gives the best overall fit. Repeating the above procedure with the rotation angles we derived for an assumed stationary India-Capricorn pole gives a slightly older best age of 8.0 Ma. The 68% (1-σ) confidence limits for these two estimates extend from 6.5 Ma to 8.7 Ma. and their 95% confidence limits extend from 5.5 Ma to 10.8 Ma.

We next sought the best model for two assumed changes in the angular rotation rate. DR Fig. 3 shows the results of a systematic search for the ages of the youngest and oldest assumed changes in motion. For each assumed age-pair shown in the figure, we inverted the India-Capricorn angles to find the three slopes and one Y-intercept that best fit the angles in a least-squares sense. Age-pairs located outside the 1-σ and 95% misfit contours (shown by the red and blue contours in the figure) are rejected at those confidence levels.

The results shown in DR Fig. 3 show that the squared misfit to the rotation angles changes significantly as a function of the age assumed for the most recent change in motion (the horizontal axis), but changes relatively little as a function of the age assumed for the earliest change in motion (the vertical axis). The change in motion at 7-8 Ma is thus well resolved by the rotation angles, whereas any change in motion before 13 Ma is poorly resolved. The improvement in fit of the best three-slope model relative to that of the best two-slope model is not significant at the 95% confidence level (as determined from an F-ratio test) for either the best-fitting sequence of angles or the stationary pole angle sequence.

The absence of evidence in the rotation angles for three distinct stages of India-Capricorn motion since 20 Ma can either be interpreted as evidence that no change occurred or as evidence that reconstructions of India-Somalia-Capricorn motion for times before 13 Ma are too noisy and too widely spaced in time to reveal any such change. As we discuss in the body of our primary paper, marine seismic data indicate that India-Capricorn convergence began between 15.4 Ma and 13.9 Ma, favoring the latter of these two interpretations.

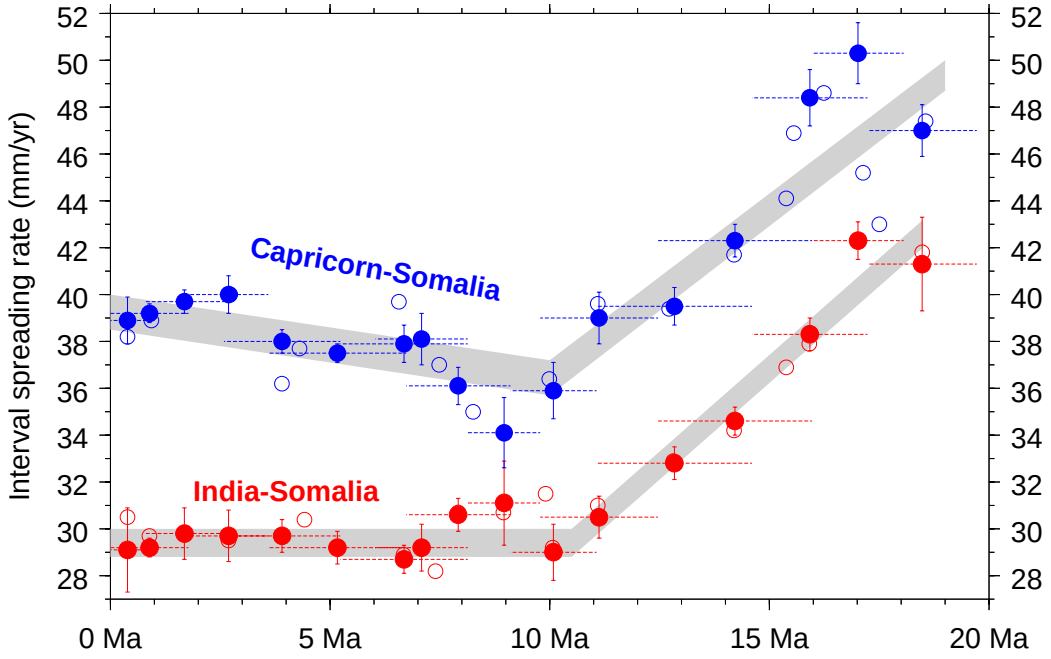

Fig. DR 1: India-Somalia and Capricorn-Somalia interval spreading rates, 0-20 Ma, updated for this analysis (solid symbols) and from *Merkouriev and DeMets* (2006) (open symbols). The updated interval rates are calculated from stage rotations determined from the rotations given in DR Table 3. Horizontal lines show the time intervals over which motion is averaged. Astronomically-tuned magnetic reversal ages are from *Husing et al.* (2007) for 0-7 Ma and 15.2-20 Ma and from *Lourens et al.* (2004) and *Husing* (2008) 7-15.2 Ma. Shaded bands are schematic interpretations of the spreading history. All rates are corrected for outward displacement.

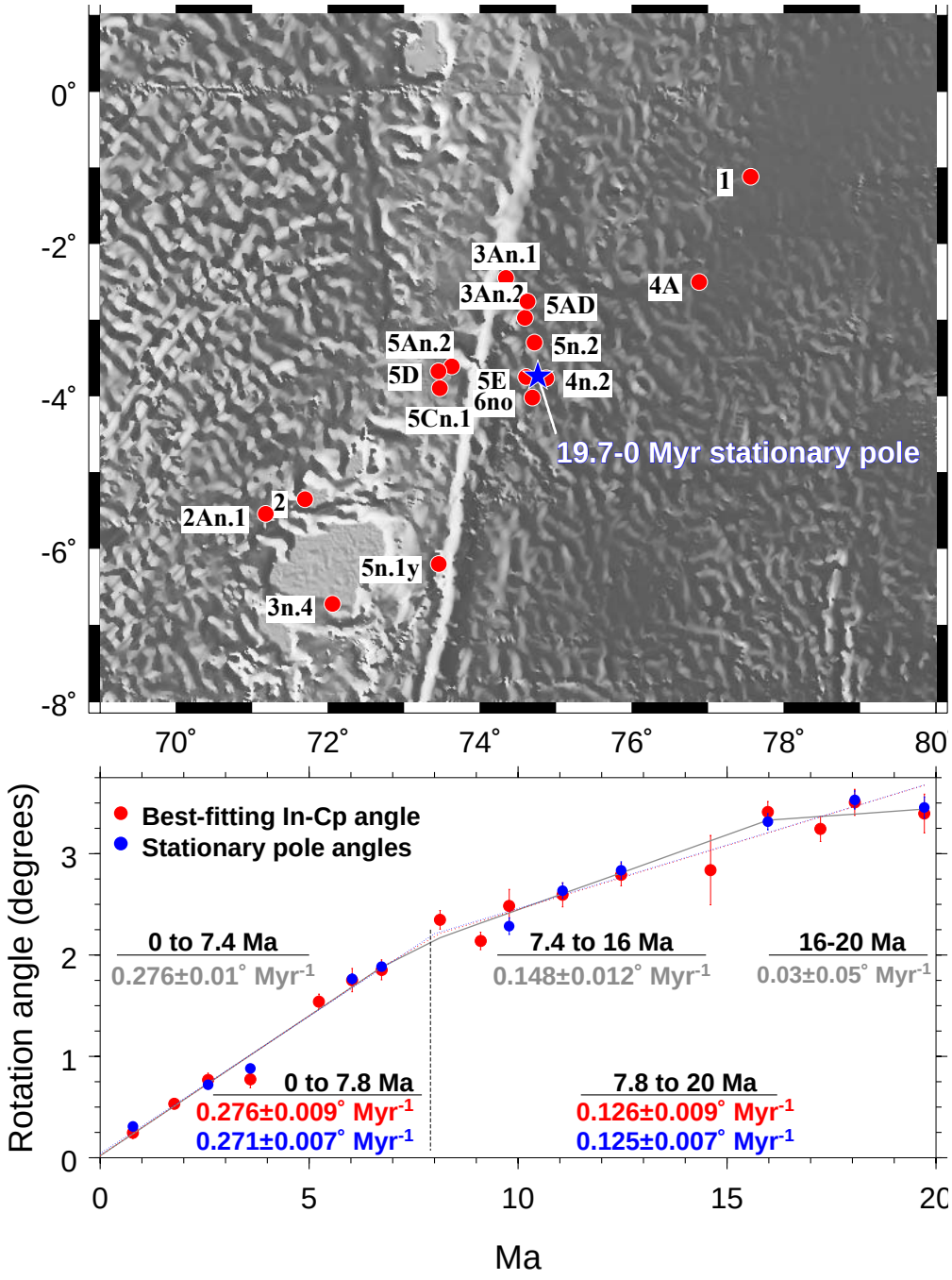

Fig. DR2: India-Capricorn pole locations for anomalies 1 (0.781 Myr) to 6n (19.722 Myr), as described in text. Blue star at 3.74^{o}S, 74.76^{o}E shows the weighted mean location of the 17 best-fitting poles from DR Table 4 (red symbols). Lower - stationary-pole and best-fitting India-Capricorn rotation angles (DR Table 4). Both sets of angles clearly show that a period of more rapid motion for the past 8 Myr was preceded by slower motion back to 16 Ma and possibly 18 Ma. Motion before ∼15 Ma may have been even slower, but cannot be resolved at statistically significant levels. Red and blue lines show continuous two-segment best-fitting lines for both sets of rotation angles. The best age (8.0 Ma) for the change in motion was determined via a systematic search for the age that gives rise to the best two-line-segment, least-squares fit to the angles. Slope uncertainties are 1-σ.

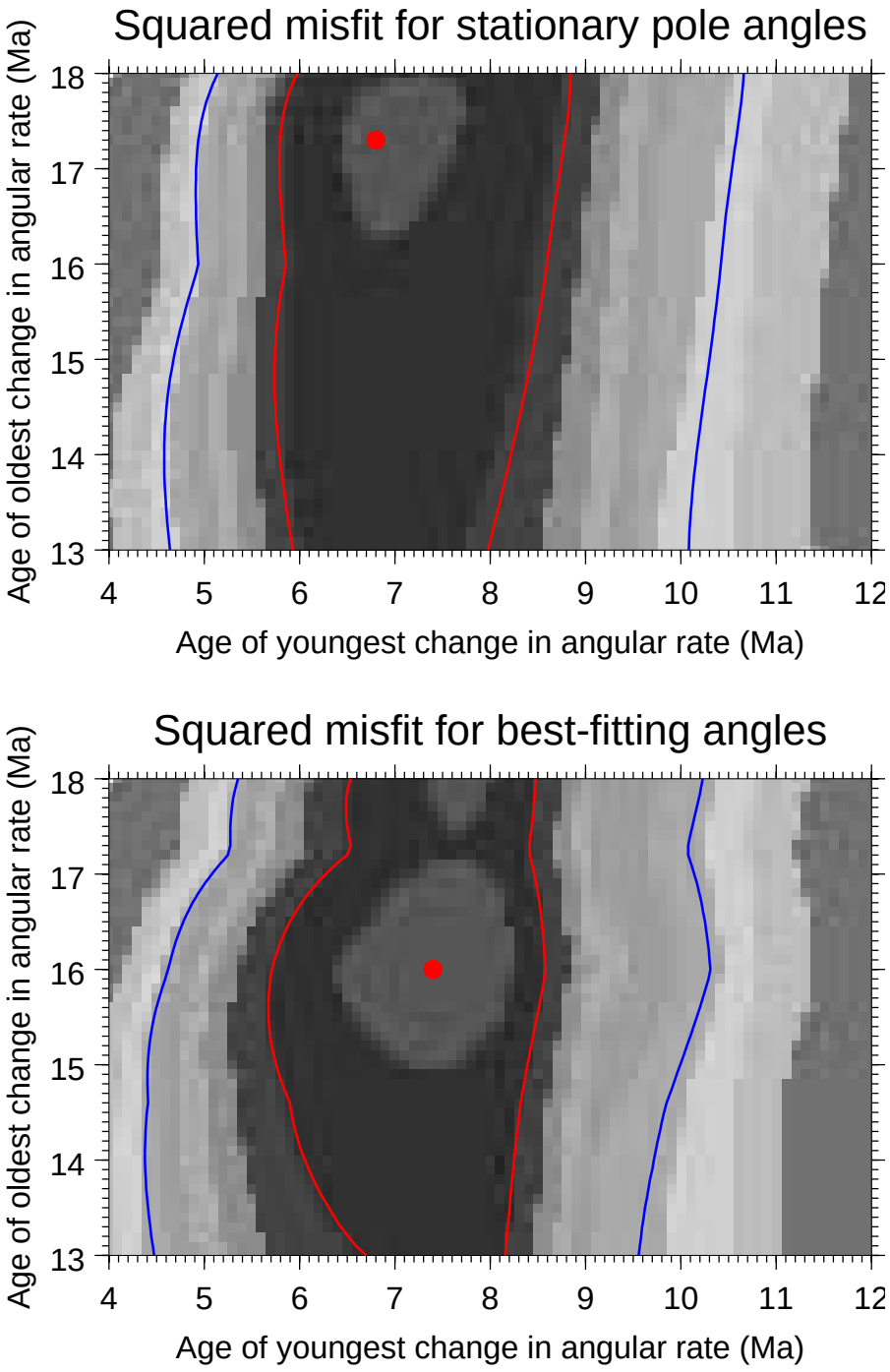

Fig. DR 3: Least-squares misfits to India-Capricorn rotation angles for two assumed changes in the rate of angular rotation, the youngest between 4 and 12 Ma and the oldest between 13 and 18 Ma. Red circles show the pair of ages that yields the lowest misfit for any 3-line-segment model to the best-fitting and stationary pole rotation angle sequences from the lower panel of DR Fig. 2. Red and blue contours show the respective 1-σ and 95% limits for the best solutions, as determined using a F-ratio test.

Papers cited

DeMets, C., & Wilson, D. S., 2008. Toward a minimum change model for recent plate motions: calibrating seafloor spreading rates for outward displacement, *Geophys. J. Int.*, **174**, 825–841, doi: 10.1111/j.1365-246X.2008.03836.x.

DeMets, C., Gordon, R. G., & Royer, J.-Y., 2005. Motion between the Indian, Capricorn, and Somalian plates since 20 Ma: implications for the timing and magnitude of distributed deformation in the equatorial Indian ocean, *Geophys. J. Int.*, **161**, 445–468.

Husing, S., 2008. Astrochronology of the Mediterranean Miocene, 171 pp., Ph. D. dissertation, Utrecht University, Utrecht, The Netherlands.

Husing, S. K., Hilgen, F. J., Abdul-Aziz, H., & Krijgsman, W., 2007. Completing the Neogene geological time scale between 8.5 and 12.5 Ma, *Earth Planet. Sci. Lett.*, **253**, 340–358, doi:10.1016/j.epsl.2006.10.036.

Lourens, L., F. J. Hilgen, J. Laskar, N. J. Shackleton, and D. Wilson (2004), The Neogene Period, in *A Geologic Time Scale 2004*, ed. F. Gradstein, J. Ogg, and A. Smith, p. 909–440, Cambridge University Press, London.

Merkouriev, S., & DeMets, C., 2006. Constraints on Indian plate motion since 20 Ma from dense Russian magnetic data: Implications for Indian plate dynamics, *Geochem. Geophys. Geosyst.*, **7, Q02002**, doi: 10.1029/2005GC001079.

Merkouriev, S., & DeMets, C., 2008. A high-resolution model for Eurasia-North America plate kinematics since 20 Ma, *Geophys. J. Int.*, **173**, 1064–1083, doi:10.1111/j.1365-246X.2008.03761.x.

Table DR1: Finite rotations for Somalia plate onto Capricorn plate

Chron	Age	Lat.	Long.	Ω	Covariances					
	Ma	^{o}N	^{o}E	(degrees)	a	b	c	d	e	f
1	0.781	11.66	51.22	0.537	10.5	12.0	-8.7	22.0	-11.0	7.6
2	1.778	10.92	49.18	1.180	24.1	19.7	-17.8	30.9	-16.4	13.8
2An.1	2.581	11.28	48.71	1.685	13.4	16.1	-10.0	27.9	-12.8	7.9
2An.3	3.596	13.71	49.62	2.238	20.6	17.4	-15.8	29.2	-13.8	12.6
3n.4	5.235	10.49	49.04	3.400	30.7	34.9	-23.4	59.8	-27.4	18.8
3An.1	6.033	12.64	48.82	3.687	54.8	60.9	-41.6	88.9	-48.1	32.7
3An.2	6.733	11.98	49.11	4.203	92.1	98.1	-71.4	120.5	-77.5	56.2
4n.2	8.132	11.62	49.74	5.114	44.4	37.3	-36.7	46.9	-31.6	31.0
4A	9.105	13.95	48.20	5.289	75.1	91.2	-55.3	142.1	-70.0	42.4
5n.1y	9.786	12.33	47.70	5.777	208.0	304.2	-136.8	497.7	-200.8	92.1
5n.2	11.067	13.99	46.84	6.258	89.6	99.9	-62.6	194.0	-74.9	46.2
5An.2	12.464	14.23	45.81	6.979	68.7	85.4	-46.9	202.9	-61.9	34.5
5AD	14.607	16.06	44.47	7.834	173.4	298.0	-118.5	588.9	-203.4	85.2
5Bn.2	15.210	16.73	43.98	8.007	234.4	390.2	-165.5	780.6	-272.7	123.2
5Cn.1	15.974	15.14	44.92	8.926	77.7	109.6	-53.3	201.6	-75.1	38.8
5Cn.3	16.721	15.66	44.48	9.331	50.3	80.0	-33.8	160.2	-54.4	24.5
5D	17.235	16.24	43.92	9.540	88.6	157.5	-56.7	314.8	-100.6	38.7
5E	18.056	16.08	44.33	10.190	97.3	149.8	-62.9	279.3	-97.6	43.0
6ny	18.748	17.38	43.33	10.309	197.0	267.3	-127.5	461.4	-177.2	86.4
6no	19.722	17.29	43.25	10.895	75.5	126.3	-50.8	259.3	-86.4	36.0

Somalia-Capricorn finite rotations from Table 3 of *DeMets et al.* (2005) interpolated to magnetic isochrons consistent with Somalia-India rotations in DR Table 2. Rotation angles are anticlockwise and reconstruct the Somalia plate onto Capricorn. Covariances are Cartesian and have units of 10^{-8} radians^2. Elements *a*, *d*, and *f* are the variances of the (0^{o}N, 0^{o}E), (0^{o}N, 90^{o}E), and 90^{o}N components of the rotation. The covariance matrices are reconstructed as follows:

$$\begin{pmatrix} a & b & c \\ b & d & e \\ c & e & f \end{pmatrix}$$

Table DR2: Finite rotations for Somalia plate onto India plate

Chron	Age	Lat.	Long.	Ω	Covariances					
	Ma	^{o}N	^{o}E	(degrees)	a	b	c	d	e	f
1	0.781	19.57	27.97	0.347	20.0	34.1	-.1	68.1	5.8	4.6
2	1.778	21.59	30.83	0.755	4.3	6.5	-.5	13.2	1.7	2.1
2An.1	2.581	22.48	30.60	1.074	30.2	43.5	-7.2	77.0	-.7	9.4
2An.3	3.596	18.70	34.62	1.642	46.6	73.8	-6.5	140.7	5.4	13.0
3n.1	4.187	22.11	28.45	1.740	44.9	72.0	-4.1	132.2	3.4	8.5
3n.4	5.235	22.05	31.64	2.181	23.0	35.9	-4.1	68.0	0.7	6.0
3An.1	6.033	22.89	28.11	2.333	74.3	117.5	-20.2	224.6	-7.7	23.4
3An.2	6.733	21.32	30.92	2.748	25.9	48.0	-1.3	95.5	2.2	4.2
4n.1y	7.554	22.61	30.57	2.982	62.7	120.8	-6.4	264.7	9.8	17.8
4n.2	8.132	22.01	30.79	3.281	50.6	82.3	-14.5	153.8	-10.7	14.1
4r.2	8.771	22.48	30.77	3.489	48.7	64.4	-17.7	133.8	8.6	29.4
4A	9.105	22.59	30.78	3.685	15.9	18.4	-7.7	37.8	2.8	12.5
5n.1y	9.786	23.59	30.49	3.890	34.0	51.2	-4.2	100.1	10.8	14.8
5n.2	11.067	23.62	29.30	4.311	49.3	75.5	-4.3	156.0	14.3	13.3
5An.2	12.464	23.80	29.26	4.879	38.6	56.2	-8.6	101.3	1.4	13.4
5AD	14.607	24.60	29.14	5.760	33.8	66.2	1.2	136.6	5.0	2.2
5Cn.1	15.974	24.80	29.30	6.399	15.3	24.5	-3.1	55.6	1.6	4.3
5D	17.235	24.83	30.29	7.149	21.5	32.0	-4.0	63.3	2.5	6.0
5E	18.056	24.77	30.27	7.637	31.6	60.6	-.2	128.2	5.1	3.4
6no	19.722	25.41	30.60	8.469	376.8	365.7	-197.7	551.9	-80.4	172.7

Somalia-India rotations modified from *Merkouriev and DeMets* (2006) as described in the text. Rotation angles are anti-clockwise and reconstruct the Somalia plate onto India. Information about the covariances is given in the footnotes to DR Table 1.

Table DR3: Rotations corrected for outward displacement

Chron	Age	Somalia-Capricorn			Somalia-India		
	(Ma)	Lat. ^{o}N	Long. ^{o}E	Ω (degrees)	Lat. ^{o}N	Long. ^{o}E	Omega (degrees)
1	0.781	10.24	52.04	0.527	17.55	32.12	.328
2	1.778	10.28	49.54	1.170	20.72	32.78	0.737
2An.1	2.581	10.84	48.97	1.675	21.90	31.96	1.055
2An.3	3.596	13.39	49.81	2.228	18.26	35.53	1.626
3n.4	5.235	10.27	49.16	3.390	21.76	32.31	2.163
3An.1	6.033	12.45	48.94	3.676	22.65	28.73	2.313
3An.2	6.733	11.81	49.21	4.193	21.09	31.45	2.730
4n.2	8.132	11.48	49.82	5.104	21.83	31.24	3.262
4A	9.105	13.81	48.29	5.279	22.44	31.18	3.666
5n.1y	9.786	12.21	47.78	5.767	23.45	30.87	3.870
5n.2	11.067	13.88	46.91	6.247	23.50	29.64	4.292
5An.2	12.464	14.13	45.87	6.967	23.69	29.56	4.859
5AD	14.607	15.98	44.53	7.823	24.51	29.40	5.740
5Cn.1	15.974	15.06	44.97	8.915	24.72	29.54	6.379
5D	17.235	16.17	43.97	9.528	24.76	30.50	7.130
5E	18.056	16.01	44.37	10.178	24.71	30.47	7.617
6no	19.722	17.23	43.29	10.883	25.35	30.78	8.450

Somalia-Capricorn and Somalia-India rotations corrected for outward displacement. Rotation angles are anti-clockwise and reconstruct the Somalia plate onto the India and Capricorn plates. Somalia-Capricorn finite rotations in DR Table 1 have been perturbed by a clockwise rotation of 0.018^o about a pole located at Ω = 55.3^oN, 5.3^oE to correct for the influence of 2 km of outward displacement along the plate boundary. Somalia-India finite rotations from DR Table 2 have been perturbed by a clockwise rotation of 0.032^o about a pole located at Ω = 32.7^oN, 330.9^oE to correct for 3.5 km of outward displacement along the Carlsberg Ridge. The rotation uncertainties are given in DR Tables 1 and 2.

Table DR4: Capricorn-India plate motion rotations

Chron	Age	Lat.	Long.	Ω	Covariances					
	Ma	^{o}N	^{o}E	(degrees)	a	b	c	d	e	f
1	0.781	1.12	77.56	-.248	30.2	46.1	-8.7	90.4	-5.1	12.3
2	1.778	5.36	71.70	-.533	27.7	26.2	-18.1	44.7	-14.8	16.0
2An.1	2.581	5.55	71.18	-.768	42.2	59.3	-16.5	106.1	-13.1	17.6
2An.3	3.596	1.02	79.64	-.772	64.3	90.5	-21.1	172.0	-7.6	26.5
3n.4	5.235	6.73	72.06	-1.541	49.8	69.8	-25.6	131.4	-26.0	25.1
3An.1	6.033	2.45	74.34	-1.752	118.5	175.5	-56.8	323.1	-54.1	57.2
3An.2	6.733	2.97	74.59	-1.854	106.0	143.6	-67.4	227.5	-76.6	60.9
4n.2	8.132	3.77	74.87	-2.348	84.2	117.5	-46.7	209.8	-42.1	46.9
4A	9.105	2.51	76.88	-2.139	78.2	106.4	-57.0	192.8	-67.9	54.9
5n.1y	9.786	6.20	73.46	-2.486	207.7	342.1	-122.5	637.7	-184.2	101.2
5n.2	11.067	3.30	74.72	-2.594	120.1	169.5	-58.3	367.4	-53.9	60.9
5An.2	12.464	3.61	73.63	-2.793	90.4	134.6	-46.7	321.7	-51.8	47.3
5AD	14.607	2.76	74.62	-2.837	162.0	335.0	-87.0	786.8	-170.9	71.4
5Cn.1	15.974	3.90	73.47	-3.411	71.8	124.4	-44.2	282.5	-64.9	39.0
5D	17.235	3.68	73.46	-3.245	81.9	171.4	-41.9	415.5	-79.3	35.5
5E	18.056	3.75	74.61	-3.507	96.5	191.4	-42.7	447.7	-72.0	38.8
6no	19.722	4.02	74.69	-3.395	341.7	475.3	-197.5	908.9	-154.4	221.5

Capricorn-India rotations determined from rotations in DR Table 3 and rotation covariances in DR Tables 1 and 2. Positive rotation angles are anti-clockwise and reconstruct the Capricorn plate onto India. Frame of reference is the India plate. Information about the covariances is given in the footnotes to DR Table 1.